

# From Cosmicflows distance moduli to unbiased distances and peculiar velocities

Yehuda Hoffman,<sup>1\*</sup> Adi Nusser,<sup>2</sup> Aurélien Valade,<sup>3,4</sup> Noam I. Libeskind,<sup>3,4</sup> R. Brent Tully<sup>5</sup>

<sup>1</sup>*Racah Institute of Physics, Hebrew University, Jerusalem 91904, Israel*

<sup>2</sup>*Physics Dept, The Technion, Haifa 32000, Israel*

<sup>3</sup>*Leibniz Institut für Astrophysik Potsdam (AIP), An der Sternwarte 16, D-144 Potsdam, Germany*

<sup>4</sup>*University of Lyon, UCB Lyon 1, CNRS/IN2P3, IUF, IP2I Lyon, France*

<sup>5</sup>*Institute for Astronomy, University of Hawaii, Honolulu HI 96822, USA*

Submitted XXXX XXX XXXX

## ABSTRACT

Surveys of galaxy distances and radial peculiar velocities can be used to reconstruct the large scale structure. Other than systematic errors in the zero-point calibration of the galaxy distances the main source of uncertainties of such data are errors on the distance moduli, assumed here to be Gaussian and thus turn into lognormal errors on distances and velocities. Naively treated, it leads to spurious nearby outflow and strong infall at larger distances. The lognormal bias is corrected here and tested against mock data extracted from a  $\Lambda$ CDM simulation, designed to statistically follow the grouped Cosmicflows-3 (CF3) data. Considering a subsample of data points, all of which have the same true distances or same redshifts, the lognormal bias arises because the means of the distributions of observed distances and velocities are skewed off the means of the true distances and velocities. Yet, the medians are invariant under the lognormal transformation. That invariance allows the Gaussianization of the distances and velocities and the removal of the lognormal bias.

This Bias Gaussianization correction (BGc) algorithm is tested against mock CF3 catalogs. The test consists of a comparison of the BGc estimated with the simulated distances and velocities and of an examination of the Wiener filter reconstruction from the BGc data. Indeed, the BGc eliminates the lognormal bias.

The estimation of Hubble's constant ( $H_0$ ) is also tested. The residual of the BGc estimated  $H_0$  from the simulated values is  $-0.6 \pm 0.7 \text{ km s}^{-1} \text{ Mpc}^{-1}$ , and is dominated by the cosmic variance. The BGc correction of the actual CF3 data yields  $H_0 = 75.8 \pm 1.1 \text{ km s}^{-1} \text{ Mpc}^{-1}$ .

## 1 INTRODUCTION

In the standard model of cosmology departures from uniform density and pure Hubble flow are strongly coupled - density irregularities induce peculiar velocities on top of the Hubble flow; peculiar velocities drive the matter away from uniform distribution. The equation of continuity tells it all (Peebles 1980; Weinberg 2008). This is why surveys of peculiar velocities of galaxies play such an important role in unveiling the underlying - luminous and dark - mass distribution in the nearby universe (Lilje et al. 1986; Lynden-Bell et al. 1988; Dekel et al. 1990; da Costa et al. 1996; Masters et al. 2006, is only a partial list). Peculiar velocity surveys have also been used to constraints cosmological parameters (e.g. Dekel et al. 1993; Zaroubi et al. 2001; Nusser & Davis 2011; Nusser 2017; Peery et al. 2018). Velocity surveys are less effective in constraining the values of cosmological parameters compared with other probes - CMB anisotropies in particular (e.g. Planck Collaboration 2014), but they are our only means for directly mapping the (total) mass distribution in the nearby universe.

Of particular interest is the Cosmicflows project<sup>1</sup> of measuring and compiling distances and redshifts of galaxies, and thereby estimating their peculiar velocities. Three data catalogs have been released so far: Cosmicflows-1 (Tully et al. 2008), Cosmicflows-2 (Tully et al. 2013) and Cosmicflows-3 (Tully et al. 2013, hereafter CF3). The Constrained Local UniversE Simulation's (CLUES) collaboration<sup>2</sup> primary focus is on the reconstruction of the present epoch density and velocity fields (e.g. Courtois et al. 2012, 2013; Tully et al. 2014; Hoffman et al. 2017; Pomarède et al. 2017, 2020) and on setting initial conditions for constrained simulations of the local universe (e.g. Hoffman et al. 2008; Forero-Romero et al. 2011; Yepes et al. 2014; Sorce et al. 2016; Hoffman et al. 2018; Ocvirk et al. 2020; ?) from the Cosmicflows data.

Theorists like peculiar velocities - their emergence in the standard cosmological model, the  $\Lambda$ CDM model, is well understood and in the linear regime the velocity and the density fields are related by a simple linear relation. This stands in sharp contrast to the dif-

<sup>1</sup> <https://www.ip2i.in2p3.fr/projet/cosmicflows>

<sup>2</sup> <https://www.clues-project.org/cms/>

difficulties arising in estimating velocities from observations. In the rest of the paper we shall focus on one particular data catalog - the CF3 data - and address various issues concerning these data that arise within the framework of the linear reconstruction of the density and 3D velocity fields from radial peculiar velocities by means of the Wiener filter and constrained realizations of Gaussian random fields (WF/CRs; Hoffman & Ribak 1991; Zaroubi et al. 1995, 1999).

The CF3 data (Tully et al. 2016) is based on the two early releases of the Cosmicflows data (Tully et al. 2008, 2013) augmented by more recently observed galaxies observed with *Spitzer Space Telescope* for which TF (Tully & Fisher 1977) distances are estimated and by the addition from the literature of the extensive Fundamental Plane (FP) sample derived from the Six Degree Field Galaxy Survey (6dFGS) of the southern celestial hemisphere (Springob et al. 2014). Tully et al. (2016) describes the different biases corrections, the homogenization of the different data sources and the zero-point calibration of the data thereby taking care of the sources of the systematic errors. Here we assume that the systematic uncertainties of the CF3 data have been properly dealt with, leaving us with the genuine statistical uncertainties that are being addressed here.

Peculiar velocities surveys are notoriously known to suffer from the so-called Malmquist bias (after Malmquist 1920, 1924), which has been extended to encompasses a variety of biases stemming from the fact that such surveys are essentially flux limited and are therefore subject to selection biases. The various aspects of the Malmquist bias have been classified as the selection, homogenous and non-homogeneous Malmquist biases (Lynden-Bell et al. 1988; Lynden-Bell 1992; Strauss & Willick 1995; Sorce 2015). There is another bias that is often being associated with the Malmquist bias - one that stems from the Gaussian errors on the distance moduli and thereby results in lognormal uncertainties on the distances. This lognormal bias skews the distribution of the observed velocities at a given observed distance shell towards negative values. Fig. 1 manifests very clearly the lognormal bias - it shows the scatter of radial peculiar velocities vs. distances, true and ‘observed’ ones, of a mock catalog drawn from a  $\Lambda$ CDM simulation (see below).

A brief and incomplete review of mostly recent attempts to correct for the Malmquist biases in velocity surveys follows. Nusser & Davis (1995) presented a method of deriving a smoothed and unbiased estimated velocity field from a survey of spiral galaxies with TF distances, based on minimizing the scatter in the inverse TF relation. Watkins & Feldman (2015) (hereafter WF15) address the bias by suggesting a new estimator of the velocity, given the redshift and estimated distance. Sorce (2015) presented a different approach to correcting the lognormal bias - a phenomenological correction to the 1-point distribution function of the velocities is introduced to eliminate the lognormal bias. The procedure was applied to the Cosmicflows-2 data set. A fully Bayesian comprehensive approach to the bias-free estimation of galaxy distances and velocities and to the (linear) reconstruction of the density and velocity fields has been recently developed (Lavaux 2016; Graziani et al. 2019). The method is based on Markov Chain Monte Carlo (MCMC) sampling of the posterior Bayesian probability distribution function and it has been applied to the CF3 data. A detailed comparison between the method presented here and the MCMC approach of Graziani et al. (2019) is to be presented elsewhere (Valade et al, in prep).

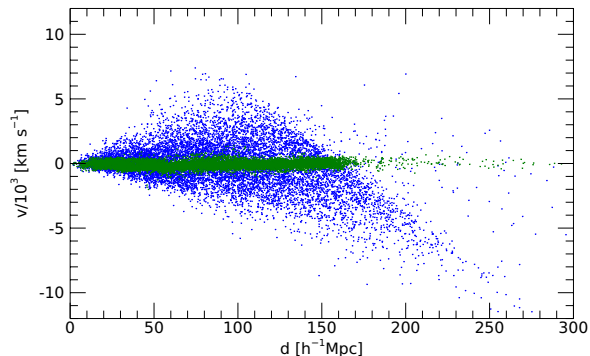


**Figure 1.** A scatter plot of radial peculiar velocities vs. distance of data points drawn from a CF3-like mock catalog. The blue symbols represent the estimated distances and velocities of the ‘observed’ data points. The actual values, drawn from the simulation, are presented for reference in green. All the different scatter plots shown in the paper are based on data drawn from one of the mock catalogs.

Application of the WF/CRs to the observed un-corrected CF3-like data so as to reconstruct the local underlying density and velocity fields would yield a very distorted structure. Consider, for example, the mock data presented in Fig. 1. A WF reconstruction would give rise to a spurious radial outflow out to a distance of  $\approx 70h^{-1}$  Mpc (where  $h = H_0/100 \text{ km s}^{-1} \text{ Mpc}^{-1}$  and  $H_0$  is Hubble’s constant) and a strong inflow beyond that. These false outflow and inflow are induced by the lognormal bias of the velocity data coupled with the given radial distribution of the data points. A close examination of how the WF works reveals that it is insensitive to sampling issues that give rise to the various aspects of Malmquist bias but is strongly affected by the lognormal bias. The aim of the present paper is to present a new scheme for correcting the lognormal bias within the framework of the WF/CRs reconstruction. This is tested here against CF3-like mock catalogs drawn from a cosmological simulation constructed within the framework of the  $\Lambda$ CDM standard model of cosmology.

The paper starts with a brief review of the CF3 data (§2) and the constructed CF3-like mock catalogs (§3). The methodology is presented in §4, and its testing against mock catalogs in §5. It is further tested in the context of the WF reconstruction from velocity surveys (§6) and of the estimation of Hubble’s constant (§8). The bias corrected actual Cosmicflows-3 catalog is presented in 9. A summary and a discussion conclude the paper (§10).

## 2 THE GROUPED COSMICFLOWS-3 DATA

Tully et al. (2016) provides a detailed account of the CF3 data. Given our interest in the linear WF/CRs reconstruction we focus here on the grouped version of the CF3 data. The grouping process collapses all galaxies that are members of a given group or a cluster into a single data point. This suppresses the virial motions within collapsed halos and thereby effectively eliminates the main source of non-linearities in the velocity field. The error of a grouped data point is the mean of the errors on the distance moduli of the mem-

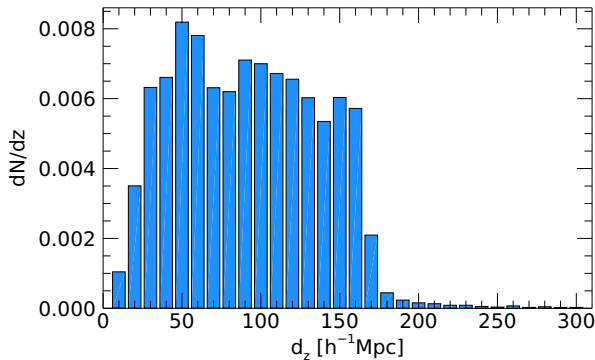


**Figure 2.** CF3 grouped data: Density of the distribution of data point with respect to their redshift distance ( $d_z = cz/H_0$ )

bers of the group reduced by the inverse of the square root of the number of the group’s members. It follows that a data point of the grouped CF3 data is either identical to that of the full CF3 data for a group of a single member or it inherits the properties of its member galaxies by taking the arithmetics mean of their redshifts and angular positions with a reduced error.

The grouping reduces the number of entries from 17,669 down to 11,501. The process suppresses the internal virial motions within groups and clusters, and thereby provides a proxy to their linear velocities. The redshift distance distribution of the data points is presented by Fig. 2. The data manifests a sharp redshift cutoff at a redshift distance of  $d_z \sim 160 h^{-1}\text{Mpc}$  ( $d_z = cz/H_0$ ), with only  $\sim 400$  galaxies that lie outside of that limit.

### 3 MOCK COSMICFLOWS-3 CATALOGS

Mock catalogs of the grouped CF3 data have been constructed so as to test the bias correction scheme presented here. The mock catalogs are drawn from the publicly available Multi-Dark-2 simulation<sup>3</sup> (Klypin et al 2016). This is a dark matter only  $N$ -body simulation with  $N = 3840^3$  in a periodic box of side length  $1.0h^{-1}\text{Gpc}$  particles of mass  $m = 1.5 \times 10^9 h^{-1}M_\odot$  with a force resolution of  $\epsilon = 5\text{ kpc}$ , assuming a Planck cosmology ( $H_0 = 67.7\text{ km s}^{-1}\text{Mpc}^{-1}$ ,  $\Omega_\Lambda = 0.69$ ,  $\Omega_b = 0.04$ ,  $\Omega_m = 0.31$ ,  $\sigma_8 = 0.82$ ) (Planck Collaboration 2014). A “Friends-of-Friends” (FOF) algorithm is run on the  $z = 0$  particle distribution and all groups larger than 20 particles are retained as halos. By design all FOF halos are ‘parent’ halos - namely ones that are not embedded in larger and more massive halos. Parent halos have substructures but are not substructure themselves.

The data points of the grouped CF3 catalog correspond to collapsed groups and clusters of galaxies, some of which are made of single galaxies. The assumption made here is that these Cf3 groups - composed of single or multiple galaxies - are associated with parent halos of the DM particles distribution. The construction of the mock grouped CF3 data is based on the pairing of the actual observed

data points with parent halos of the simulation, retaining their observed positions in redshift space and their errors. Thus, the mock data points are ‘ignorant’ of the grouping of the actual CF3 galaxies other than inheriting the errors of the grouped CF3 data points that are strongly affected by the grouping. It follows that the issue of grouping is left out of the discussion here and it is assumed to be done prior to the analysis presented in the paper.

The construction starts with selecting a Milky Way mass halo as the mock LG, namely, one halo with mass  $9 \times 10^{11}M_\odot < M_{\text{cen}} < 2 \times 10^{12}M_\odot$  (out of 3,333,049 possibilities) is randomly chosen to host the mock observer. Using the periodicity of the simulation, all haloes are centered on the mock observer. A Supergalactic-like cartesian coordinate system aligned with the computational box and centered on the mock LG, is then constructed with the (SGX, SGY, SGZ) orientation randomly selected.

The procedure aims at pairing simulated halo with CF3 data points, while minimizing their separation distances in redshift space. This is done in two steps, per each CF3 data point. Halos are then projected on to the mock sky, and are binned in Supergalactic (SGL, SGB) bins. All the halos in the angular bin of a given CF3 data point are identified, and among them the halo closest in redshift to the observed redshift is selected for the mock catalog. The estimated errors of the CF3 data are assigned to their mock counterparts.

The algorithm of generating mock catalogs includes the application of the Friedmann-Robinson-Walker (FRW) metric to the otherwise Newtonian variables of the numerical code, turning Newtonian spatial coordinates into luminosity distances and the simple Newtonian peculiar velocities into the ones actually observed in an FRW universe.

Ten different mock observers have been randomly selected and ten different errors realizations have been constructed yielding 100 different mock catalogs altogether. The ten different observers sample the cosmic variance of CF3-like surveys and the ten errors realizations sample the error variance associated with the observational uncertainties associated with the individual measurements of individual data points. All the different scatter plots shown in the paper are based on data drawn from one of these mock catalogs.

## 4 METHODOLOGY

### 4.1 Basics

Peculiar velocity surveys/catalogs consist of the luminosity distance,  $d_L$ , the observed redshift,  $z$ , angular position and the errors associated with the luminosity distance and the redshift of a collection of data points. All the steps involved in extracting proper distances ( $d$ ) and peculiar radial velocities ( $v$ ) from Cosmicflows-like data are briefly presented here. The following derivation is given here for the sake of completeness (see Weinberg 2008; Davis & Scrimgeour 2014).

In a flat universe the cosmological redshift  $z_{\text{cos}}$  of the luminosity

<sup>3</sup> see <https://www.cosmosim.org>

distance are related by:

$$d_L = cH_0^{-1}(1 + z_{\text{cos}}) \int_0^{z_{\text{cos}}} \frac{1}{\sqrt{\Omega_m(1+z)^3 + (1-\Omega_m)}} dz \quad (1)$$

(here  $c$  and  $\Omega_m$  are the speed of light, and the cosmological matter density parameter, respectively). Eq. 1 is solved to find  $z_{\text{cos}}$  for a given  $d_L$  and a given cosmology ( $H_0$  and  $\Omega_m$ ). The proper distances ( $d$ ) is given by:

$$d = \frac{d_L}{(1 + z_{\text{cos}})} \quad (2)$$

The observed redshift of an object is related to its cosmological redshift and peculiar radial velocity ( $v$ ) by,

$$1 + z = (1 + z_p)(1 + z_{\text{cos}}), \quad (3)$$

where  $z_p = v/c$ . Eq. 3 is used to calculate  $v$ . A 1st order expansion of Eq. 3 yields the familiar expression,

$$cz \sim H_0 d + v. \quad (4)$$

For the vast majority of the galaxies in the CF3 catalog - e.g. spirals with Tully-Fisher distances and ellipticals with FP distances - distance estimation from observables starts with the distance moduli ( $\mu$ ). It is related to the (luminosity) distance by

$$\mu = 5 \log_{10} \left( \frac{d_L}{10 \text{ pc}} \right) \quad (5)$$

For mathematical convenience Eq. 5 is rewritten as

$$\mu = B \ln \left( \frac{d_L}{A} \right) \quad (6)$$

where  $B = 5/\ln 10$  and  $A = 10 \text{ pc}$ .

It is commonly assumed that errors on the observed distance modulus are normally distributed,  $\mu_{\text{obs}} = \mu + \sigma_\mu \epsilon$ , where  $\epsilon \in \mathcal{N}(0, 1)$  (namely, normal distribution of zero mean and variance of unity). It follows that the ‘observed’ luminosity distance is

$$D_L = A \exp\left(\frac{\mu_{\text{obs}}}{B}\right) = A \exp\left(\frac{\mu + \sigma_\mu \epsilon}{B}\right) \quad (7)$$

A first order expansion of the observed with respect to the true proper distances, namely  $D$  with respect to  $d$ , yields:

$$D \approx d(1 + \tilde{\sigma}_\mu \epsilon) \quad (8)$$

where  $\tilde{\sigma}_\mu = \sigma_\mu/B$ . Here  $d$  and  $D$  are the true and observed proper distances of a data point, respectively. It is noted here that the distance measurement errors scale with true and not with the observed distance. The typical uncertainty in the TF relation for a field spiral is  $\sigma_\mu \sim 0.4$  resulting in fractional (TF) distance uncertainty of  $\sim 0.18$ . The observational uncertainty on the derived velocity,  $\epsilon_v$  is closely related to the distance uncertainty,

$$\epsilon_v = -H_0 d \tilde{\sigma}_\mu \epsilon. \quad (9)$$

Here the  $50 \text{ km s}^{-1}$  uncertainties on the redshifts are neglected.

The normal distribution of the distance modulus errors and the exponential dependence of the distance on the distance modulus imply that the distance and the velocity errors are lognormal distributed. Hence the distance and velocity estimations are biased. Namely, even in the limit of infinite many repeated observations of a give galaxy the means of the estimated distances and velocities do not coincide with their actual values.

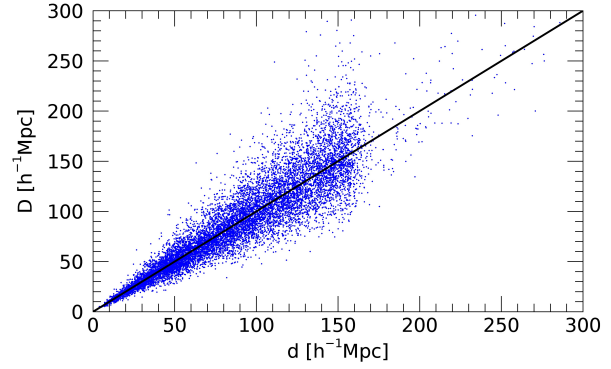


**Figure 3.** A scatter plot of the observed ( $D$ ) vs the actual ( $d$ ) distances drawn from a CF3-like mock catalog.

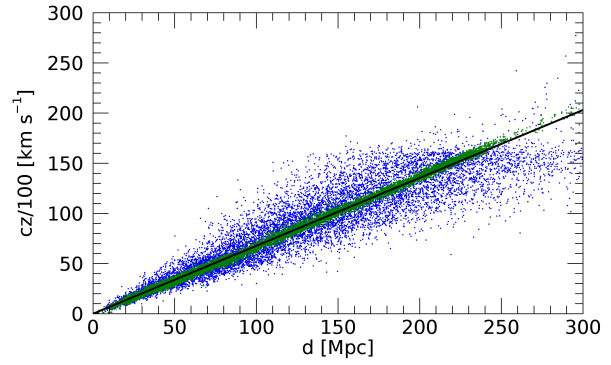


**Figure 4.** A Hubble diagram, namely  $cz$  vs. distance, is drawn for one of the mock catalogs. Distances are given in Mpc, taking the actual  $H_0^{\Lambda\text{CDM}} = 67.7 \text{ km s}^{-1} \text{ Mpc}^{-1}$  of the simulation. Blue symbols correspond to observed data points and green ones for the actual, values. The solid line corresponds to the Hubble velocity-distance law.

The exponential dependence of the distance on the distance modulus makes the distribution of the estimated errors skewed (Fig. 3). That bias affects the distribution of the estimated peculiar velocities with respect to their estimated distances in two ways - it changes the spatial distribution of the data points and the actual values of the estimated velocities. This is clearly depicted by Fig. 1 which shows the distribution of velocities and distances of the observed mock data points. The bias affects also a Hubble diagram constructed from the mock catalog, namely  $cz$  vs the distances of the mock data. Eq. 4 implies that a small scatter is expected even for the ‘clean’ (i.e zero errors) data, as a consequence of the emergence of peculiar velocities associated with structure formation out of a primordial density perturbation field (Fig. 4). For the standard  $\Lambda\text{CDM}$  model assumed here the expected scatter is roughly  $\sigma_{vp} \sim 275 \text{ km s}^{-1}$  (for the radial component of the velocity as is calculated from the simulated mock catalogs).

In the standard model of cosmology peculiar velocities are assumed to constitute a random (vector) Gaussian field defined by the primordial power spectrum. Non-linear dynamics and in particular

virial motions in collapsed groups and clusters of galaxies violate the prediction of the linear theory of structure formation. Grouping the CF3 catalog suppresses the non-linear motions and acts as an effective linearization of the observed velocities. It follows that radial velocities are expected to scatter normally as a function of their distance from a random observer in a  $\Lambda$ CDM universe. Fig. 1 shows the scatter of actual  $v$  vs  $d$  and of observed  $V$  vs  $D$  for one of the mock catalogs. The bias is very clearly manifested.

## 4.2 Distances

We first consider an ideal case of a subsample of data points all of which have the same actual distance ( $d$ ) but different observed distances ( $D$ ). The lognormal probability distribution function (PDF) of the observed given the actual distances is given by

$$P(D|d) = \frac{1}{\sqrt{2\pi}\tilde{\sigma}_\mu} \exp\left(-\frac{(\ln(D/d))^2}{2\tilde{\sigma}_\mu^2}\right) \frac{1}{D}. \quad (10)$$

Given the lognormal PDF (Eq. 10) one finds that the median, mean, variance and standard deviation of  $D$  given  $d$  are easily calculated:

$$\begin{aligned} (D|d)_{med} &= d \\ \langle D|d \rangle &= d \exp\left(\frac{\tilde{\sigma}_\mu^2}{2}\right) \\ \langle D^2|d \rangle &= d^2 \exp(2\tilde{\sigma}_\mu^2) \\ \sigma_D &= d \sqrt{\exp(2\tilde{\sigma}_\mu^2) - \exp(\tilde{\sigma}_\mu^2)} \end{aligned} \quad (11)$$

Here  $\sigma_D^2$  is the central moment of  $D$  given  $d$ .

The value of  $d$  can be estimated from the subsample by recalling that median of  $D$  equals the actual distance (Eq. 11). It follows that  $(D|d)_{med}$  is the distance estimator for all observed distances  $D$ . Eq. 10 is now rewritten as:

$$P(D|d) = \frac{1}{\sqrt{2\pi}\tilde{\sigma}_\mu} \exp\left(-\frac{(\ln D/(D|d)_{med})^2}{2\tilde{\sigma}_\mu^2}\right) \frac{1}{D}, \quad (12)$$

Expressing  $D$  in terms of  $\epsilon$  and recalling Eqs. 6 and 7 one writes:

$$\epsilon(D) = \frac{1}{\tilde{\sigma}_\mu} \ln\left(\frac{D}{(D|d)_{med}}\right) \quad (13)$$

The true distance,  $d$ , is unknown, but the redshift distance, defined here as  $d_z = cz_{obs}/H_0$ , is very accurately determined, and therefore we seek to replace the former by the latter:

$$\begin{aligned} P(d, d_z) &= P(d_z|d)P(d) \\ &= P(d|d_z)P(d_z), \end{aligned} \quad (14)$$

where  $P(d)$  is the probability of finding a data point in an interval  $dd$ ,  $P(d) dd = n(d)$ , where  $n(d)$  is the number of data points in that interval.  $P(d_z)$  is similarly defined,  $P(d_z) dd_z = n(d_z)$ . The derivations and discussion that follow strictly apply to the case of the grouped CF3 data where  $P(d_z) \approx const.$  over the range of  $30 \lesssim d_z \lesssim 160 h^{-1} \text{Mpc}$  (see Fig. 2). This should also be the case for  $P(d)$  given that over that range  $(d - d_z)_{rms} \approx 2.75 h^{-1} \text{Mpc}$ . Indeed, the analysis of the mock CF3 data that follows corroborates this assumption.

It follows that

$$P(d|d_z) \approx P(d_z|d). \quad (15)$$

From here on this approximate relation is taken as an equality.

Next, Eq. 12 is rewritten here as the conditional probability of  $D$  given the redshift distance:

$$\begin{aligned} P(D|d_z) &= \int P(D|\tilde{d})P(\tilde{d}|d_z) d\tilde{d} = \\ &= \frac{1}{\sqrt{2\pi}\tilde{\sigma}_\mu D} \frac{H_0}{\sqrt{2\pi}\sigma_{vp}} \int \exp\left(-\frac{(\ln(D/(D|\tilde{d})_{med}))^2}{2\tilde{\sigma}_\mu^2}\right) \\ &\quad \exp\left(-\frac{(\tilde{d} - (D|z)_{med})^2}{2(\sigma_{vp}/H_0)^2}\right) d\tilde{d}. \end{aligned} \quad (16)$$

(Here  $\tilde{d}$  is an integration variable.)

In the limit where  $\sigma_{vp} \ll cz$  the following holds,

$$P(D|d_z) = \frac{1}{\sqrt{2\pi}\tilde{\sigma}_\mu} \exp\left(-\frac{(\ln D/(D|z)_{med})^2}{2\tilde{\sigma}_\mu^2}\right) \frac{1}{D}, \quad (17)$$

The following analytical derivations are made under that assumption. In particular, Eq. 13 is rewritten here as

$$\epsilon(D) = \frac{1}{\tilde{\sigma}_\mu} \ln\left(\frac{D}{(D|z)_{med}}\right). \quad (18)$$

Our aim here is to map the lognormal distributed  $D$  to an estimator,  $d_{BGc}$  where BGc stands for bias gaussianization correction, that is normally distributed around the actual distance,  $d$ , with an unspecified yet dispersion of  $\sigma_d$ . Namely,

$$P(d_{BGc}|d_z) = \frac{1}{\sqrt{2\pi}\sigma_d} \exp\left(-\frac{(d_{BGc} - (D|z)_{med})^2}{2\sigma_d^2}\right). \quad (19)$$

Given the lognormal transformation from the true to the observed distance, the cumulative distribution of  $D$  (Eq. 10) equals to that of  $d$  (Eq. 19). It follows that the following approximate equality determines  $d_{BGc}$ :

$$\frac{1}{\sqrt{2\pi}} \int_{-\infty}^{\epsilon(D)} \exp\left(-\frac{\epsilon^2}{2}\right) d\epsilon = \int_0^{d_{BGc}} P(\tilde{d}_G|d_z) d\tilde{d}_G, \quad (20)$$

where the PDF in the integrand of the RHS of the equation is given by Eq. 19. Over the vast majority of the CF3 data points the RHS of Eq. 20 can be very well approximated by:

$$\begin{aligned} \frac{1}{\sqrt{2\pi}} \int_{-\infty}^{\epsilon(D)} \exp\left(-\frac{\epsilon^2}{2}\right) d\epsilon = \\ \frac{1}{\sqrt{2\pi}\sigma_d} \int_{-\infty}^{d_{BGc}} \exp\left(-\frac{(\tilde{d}_G - (D|z)_{med})^2}{2\sigma_d^2}\right) d\tilde{d}_G, \end{aligned} \quad (21)$$

The solution of Eq. 21 is trivial,

$$\text{erf}\left(\frac{1}{\sqrt{2}\tilde{\sigma}_\mu} \ln\left(\frac{D}{(D|z)_{med}}\right)\right) = \text{erf}\left(\frac{d_{BGc} - (D|z)_{med}}{\sqrt{2}\sigma_d}\right) \quad (22)$$

where  $\text{erf}(x)$  is the error function. It follows that

$$d_{BGc} = (D|z)_{med} + \frac{\sigma_d}{\tilde{\sigma}_\mu} \ln\left(\frac{D}{(D|z)_{med}}\right). \quad (23)$$

Eq. 17 is derived under the assumption that the PDF of the peculiar velocities of the data points is Gaussian. This is the standard assumption of the  $\Lambda$ CDM model as far as the velocity field of the DM particles is concerned. Yet, the sampling of the velocity field

by collapsed groups of the CF3 galaxies leads to non-linear coupling between the density and velocity fields, and this might lead to deviations from a Gaussian distribution. The construction of the mock data by associating the grouped CF3 data with parent halos of the DM particles distribution properly addresses this concern. An inspection of the PDF of the velocities of the mock data points shows that it is very well approximated by a Gaussian.

### 4.3 Peculiar Velocities

Again, we start here with a subsample of data points of a given true distance,  $d$ . Eq. 4 is assumed here and the observed peculiar velocity ( $V$ ) is

$$V = cz - H_0 D \quad (24)$$

(to 1st order in  $v/cz$ ).

Given the lognormal PDF (Eq. 10) and similarly to Eq. 12 one finds that the median, mean, variance and standard deviation of  $V$  given  $d$  are easily calculated:

$$\begin{aligned} (V|d)_{med} &= cz - H_0 d \\ \langle V|d \rangle &= cz - H_0 d \exp\left(\frac{\tilde{\sigma}_\mu^2}{2}\right) \\ \sigma_V &= H_0 d \sqrt{\exp(2\tilde{\sigma}_\mu^2) - \exp(\tilde{\sigma}_\mu^2)} \end{aligned} \quad (25)$$

Here  $\sigma_V^2$  is the central moment of  $V$  given  $d$ . It depends on the unknown true distance but it can be approximated by

$$\sigma_V \sim cz \sqrt{\exp(2\tilde{\sigma}_\mu^2) - \exp(\tilde{\sigma}_\mu^2)}. \quad (26)$$

A 1st order expansion yields

$$\sigma_V \sim cz \tilde{\sigma}_\mu. \quad (27)$$

The median of the observed velocities,  $(V|d)_{med}$ , and of the distances of the subsample are related by:

$$(V|d)_{med} = cz - H_0 (D|d)_{med} = cz - H_0 d \quad (28)$$

It follows that  $(V|d)_{med} = v$  (the actual peculiar velocity). The errors on the distance lead to errors on the velocities by

$$V = (V|d)_{med} - H_0 d (\exp(\tilde{\sigma}_\mu) - 1). \quad (29)$$

Replacing the ensemble of data points to one of a given redshift and under the assumption that the distance errors (scaled by  $H_0$ ) are much larger than  $\sigma_{vp}$ ,  $H_0 d$  is replaced by  $cz$  in Eq. 29. The normal error variable ( $\epsilon$ ) is related to the observed velocity by:

$$\begin{aligned} \epsilon(V) &= \frac{1}{\tilde{\sigma}_\mu} \ln\left(\frac{cz - V}{cz - (V|z)_{med}}\right) \\ &= \frac{1}{\tilde{\sigma}_\mu} \ln\left(\frac{D}{(D|d)_{med}}\right), \end{aligned} \quad (30)$$

where  $V = cz - H_0 D$ .

Given the lognormal nature of the errors on the observed velocities we introduce a Gaussian estimator of the velocity,  $v_{BGc}$ , which scatters normally around the median with a dispersion that equals

the errors of the observed velocities. Namely, the PDF of  $v_{BGc}$  is

$$P(v_{BGc}|z) = \frac{1}{\sqrt{2\pi}\sigma_V} \exp\left(-\frac{(v_{BGc} - V_{med})^2}{2\sigma_V^2}\right) \quad (31)$$

The velocity equivalent to Eq. 20 is

$$\frac{1}{\sqrt{2\pi}} \int_{-\infty}^{\epsilon(V)} \exp\left(-\frac{\epsilon^2}{2}\right) d\epsilon = \int_{-\infty}^{v_{BGc}} P(\tilde{v}_G|z) d\tilde{v}_G, \quad (32)$$

whose solution is again trivially given by

$$2 - \operatorname{erfc}\left(\frac{1}{\tilde{\sigma}_\mu} \ln\left(\frac{cz - V}{cz - (V|z)_{med}}\right)\right) = \operatorname{erfc}\left(\frac{v_{BGc} - (V|z)_{med}}{2\sigma_V}\right), \quad (33)$$

or

$$v_{BGc} = (V|z)_{med} + 2\sigma_V \operatorname{erfc}^{-1}\left(2 - \operatorname{erfc}\left(\frac{\ln\left(\frac{cz - V}{cz - (V|z)_{med}}\right)}{2\tilde{\sigma}_\mu}\right)\right) \quad (34)$$

Here  $\operatorname{erfc}(x)$  is the complimentary error function and  $\operatorname{erfc}^{-1}(x)$  is its inverse.

Given that Eq. 4 holds also for the medians of the distribution of  $D$  and  $V$ , at a given redshift, namely that

$$cz = H_0 (D|z)_{med} + (V|z)_{med}, \quad (35)$$

and recalling that  $\operatorname{erfc}^{-1}(2 - \operatorname{erfc}(x)) = -x$ , Eq. 34 is rewritten as:

$$v_{BGc} = (V|z)_{med} - \frac{\sigma_V}{\tilde{\sigma}_\mu} \ln\left(\frac{D}{(D|z)_{med}}\right) \quad (36)$$

A comforting relation that emerges from Eqs. 23 and 36 is the redshift, distance and velocity relation is valid also for the mean of the BGc estimated distances and velocities at a given redshift:

$$H_0 \langle (d_{BGc}|z) \rangle + \langle (v_{BGc}|z) \rangle = cz. \quad (37)$$

Namely, Eq. 37 is the Gaussian equivalent of the non-Gaussian Eq. 28.

### 4.4 Bias Gaussianization correction: practical implementation

A key element in the expressions for  $d_{BGc}$  and  $v_{BGc}$  is the evaluation of the medians of the observed distances and velocities for a given redshift ( $(D|z)_{med}$  and  $(V|z)_{med}$ ). This depends on a construction of a subsample of data points with redshifts close enough to  $z$ . The following reasoning is used to construct such a subsample. Define the redshift range of the data points where: a. the observed radial velocities and the residual of redshift distances from the true ones are dominated by the distance measurements errors; b. the sampling in redshift is dense enough. A given data point within that range is considered here. A subsample of  $N_z$  data points adjacent to it in their redshifts - the closest in redshifts  $N_z/2$  data points smaller than  $z$ , and likewise for the ones larger than  $z$ . The medians of the distances and velocities are constructed for that particular data point. Eqs. 23 and 36 are used to evaluate the Gaussianized estimators  $d_{BGc}$  and  $v_{BGc}$ , based on the medians evaluated for that particular data point. The procedure is repeated to all the data

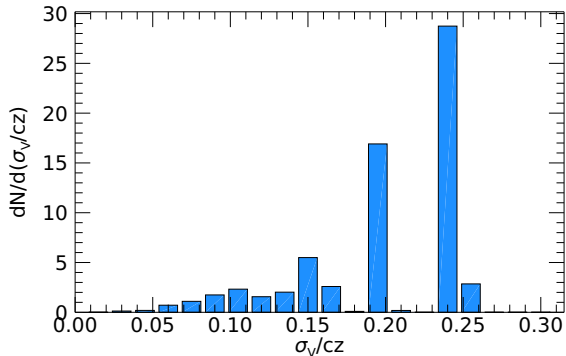


**Figure 5.** CF3 data points: Density of the distribution of data point with respect to their fractional distance errors.

point within that redshift range. The key assumption made here, upon which the BGc algorithm is built, is that for the data points within that range and their associated subsample the residual between observed and true distances and velocities are dominated by uncertainties, i.e. ‘errors’, on the distance moduli and that these are uncorrelated. It is this statistical independence of the errors on  $\mu$  which enables one to construct the subsample by their proximity in redshift regardless of their distances in the 3D redshift space.

For the case of the CF3 data and the  $\Lambda$ CDM model this range corresponds to  $15 \lesssim d_z \lesssim 160 h^{-1} \text{Mpc}$ . The lower bound is derived under the assumption that  $\sigma_{vp} \sim 275 \text{ km s}^{-1}$  and that for the nearby data points  $\langle \tilde{\sigma}_\mu \rangle \sim 0.19$ , or  $\langle d_z H_0 \tilde{\sigma}_\mu \rangle \sim 285 \text{ km s}^{-1}$ . As for the upper bound, the sampling below  $d_z \lesssim 160 h^{-1} \text{Mpc}$  is roughly uniform and is relatively extremely sparse beyond it (Fig. 2). For the data points outside that range the following is applied: a. for the nearby data points the observed distances and velocities are retained; For the few distant data points observed distances are replaced by their redshift distances and their velocities are retained.

To the extent that the data is composed of galaxies or groups of galaxies of a given redshift and all have the same fractional errors then Eqs. 23 and 36 provide accurate BGc estimations of the distances and velocities of the data points. However, this is not the case with the actual CF3 survey, where the two major subsets of data have fractional distance errors of  $\tilde{\sigma}_\mu \sim 0.18$  (TF galaxies) and  $\sim 0.24$  (6dF FP galaxies) (Fig. 5). The grouping of the data adds an additional scatter to the distance errors. It follows that Eqs. 23 and 36 are only approximately correct - an approximation that is used in the rest of the paper. We have found here that the best - in the sense discussed below - BGc estimation is obtained here by replacing the actual values of  $\tilde{\sigma}_\mu$  of individual data points by their mean value of  $\tilde{\sigma}_\mu = 0.19$ .

The BGc estimated distances are obtained by the adding a normally distributed term to the median  $(D|z)_{med}$  normalized by  $\sigma_d/\tilde{\sigma}_\mu$  (Eq. 23). The normally distributed term keeps the median and the mean of the distribution of  $d_{BGc}$  invariant and roughly equal. We take here  $\sigma_d = 0$  and thereby minimize the scatter of the BGc around the redshift distances to its minimal value of  $\sim \sigma_{vp}/H_0$ .

## 5 APPLICATION TO CF3 MOCK CATALOGS

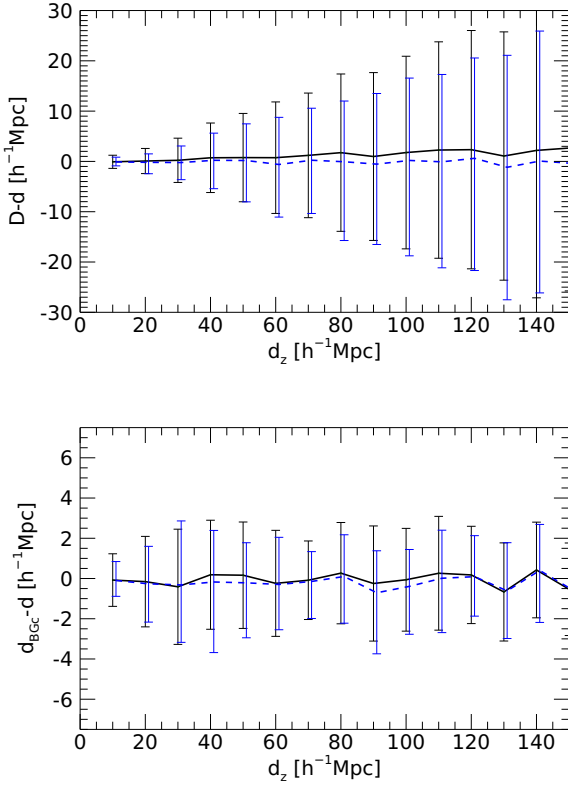
The BGc procedure is examined here for one of the mock catalogs. The results are representative of all the other mock data sets.

Fig. 6 shows the residual of the observed distances from the true ones ( $D - d$ ) vs their redshift distances (upper panel). The difference between the mean and the median of the distribution is a clear manifestation of the lognormal bias. The lower panel presents the residual of the BGc distances from the true ones. The mean and the median are virtually identical and they both oscillate around the null residual, as is expected from an unbiased Gaussian distance estimator. Likewise, Fig. 7 shows the residual of the observed from the true velocities ( $V - v$ ) and of  $(v_{BGc} - v)$  against  $d_z$ , and of the BGc estimated from the true velocities ( $v_{BGc} - v$ ) vs  $d_{BGc}$ . Again, the later case is consistent with an unbiased Gaussian distribution. There is one striking difference between the BGc correction of the distances and of the velocities. The BGc corrected distances are assumed to be normally scattered around  $(D|z)_{med}$  with a constant scatter of  $\sim \sigma_{vp}/H_0 \sim 2.75 h^{-1} \text{Mpc}$ . In contrast the BGc velocities are assumed to be normally scattered around their corresponding median with the estimated error of the uncorrected data,  $\sigma_V \sim cz \tilde{\sigma}_\mu$ .

Fig. 8 presents the distribution of the observed velocities vs their observed distances (upper panel). The lognormal bias of the distances and velocities is clearly manifested here - the mean and median are different and both deviate significantly from zero. A naive reconstruction from such a data would show strong false outflow (out to  $D \sim 100 h^{-1} \text{Mpc}$ ) and inflow (beyond it). The lower panel presents the scatter of the BGc velocities vs the BGc distances. The mean and the median are effectively identical and both oscillate around zero, as expected from a Gaussian random field.

## 6 WIENER FILTER RECONSTRUCTION: COMPARISON

The aim here is to test the BGc estimation within the context of the WF reconstruction. The WF is the optimal estimator in the case where the data is drawn from an underlying random Gaussian field and observational ‘errors’ that are normally distributed (Zaroubi et al. 1995). The case of the grouped Cosmicflows data is challenging for the WF - distances and velocities are subjected to lognormal uncertainties, yet the underlying velocity field is ‘almost’ Gaussian. Accordingly, the following ‘ideal’ mock data is constructed here - one in which the distances are known exactly and the ‘observed’ velocities are subjected to Gaussian errors given by Eq. 9 to generate the errors, with the same realization of the normal distribution used to generate the observed distance moduli. We call it here the  $V_{Gauss}$  data and it is the aim of the BGc algorithm to recover it from the lognormal data. The BGc is tested here by comparing the WF reconstruction from the  $v_{BGc}$  with the target WF from the  $V_{Gauss}$ . A good agreement among the two reconstructions means that the BGc indeed removes the lognormal bias successfully. The actual velocity field of the simulation is presented here as well. It is evaluated here by means of a clouds-in-cells (CIC) interpolation applied to the particles distribution over a grid of  $128^3$  cells covering a box of side length of  $500 h^{-1} \text{Mpc}$ . The CIC velocity field is further Gaussian smoothed with a  $5 h^{-1} \text{Mpc}$  Gaussian kernel, so



**Figure 6.** Mean (black, solid line) and median (blue, dashed line) of the residual of the observed distances ( $D$ ) (top panel) and of the estimated distances ( $d_{BGc}$ ) (lower panel) from the actual distances ( $d$ ) vs the redshift distances ( $d_z$ ) for the mock data points. Note the different vertical scales of the plots. (Black error bars correspond to one standard deviation around the mean value and the blue ones to the 1st and 3rd quartiles around the median, rescaled to correspond to the standard deviation of a normal distribution. The blue error bars are slightly shifted horizontally.)

as to suppress some of the non-linear components of the velocity and to enable a comparison with the linear WF reconstruction. The nonuniform and anisotropic sampling of the data and the observational uncertainties that increase with distance implies that even for the  $V_{Gauss}$  case the quality of the WF reconstruction is expected to degrade with distance.

Fig. 9 depicts the WF reconstruction from the  $V_{Gauss}$  data and the Gaussian smoothed CIC flow field. It further shows the WF reconstruction from the BGc estimated data and its residuals from the target  $WF/V_{Gauss}$  field. The mock Supergalactic Plane of the velocity fields is shown here. This is relevant for the distribution of the data points, which follows that of the actual CF3 data, but is inconsequential as far as the target simulation is concerned. Note the different arrow lengths for the magnitudes of the streamlines of  $WF/V_{BGc}$  and its residual. The ratio of the mean of the norm of the residual velocity field to the mean of norm of the velocity of the target field ranges from  $\sim 0.25$  to  $\sim 0.20$  within  $R = 50$  and  $150h^{-1}\text{Mpc}$  (respectively). Visual inspection of the residual velocity field does not find any clear coherence between the residual and target fields within the plane and in any case the magnitude of the residual field gets smaller by more than 20% at large distances. This is further inspected by evaluating the multipole moments of the velocity fields.

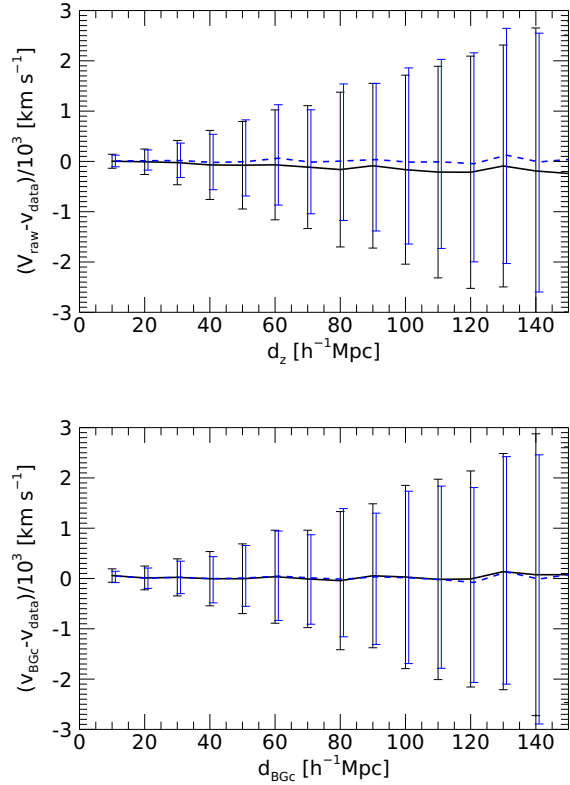


**Figure 7.** Mean (black, solid line) and median (blue, dashed line) of the residual of the observed velocity ( $V$ ) from the true velocity vs the observed distance ( $D$ , upper panel) and the residual of the estimated velocity ( $v_{BGc}$ ) from the true data vs the estimated distance ( $d_{BGc}$ , lower panel). (Same notations as in Fig. 6.)

A further insight into the large scale behaviour of the WF reconstruction is provided by the volume-weighted mean monopole and dipole moments of the velocity field in spheres of radius  $R$ . The monopole moment is the mean of  $-\nabla \cdot \vec{v}/H_0$ , where the scaling by  $H_0$  is introduced so as to make the expression dimensionless and proportional to the mean (linear) over-density within  $R$ . The minus sign is introduced so as to make the monopole within a sphere of  $R$  to be proportional to the mean over-density within that volume. It corresponds also to the local fractional perturbation to  $H_0$ . The dipole is the volume weighted mean velocity within  $R$ , i.e. the bulk velocity  $V_{bulk}(R)$ . Fig. 10 presents the monopole and dipole moments, as a function of  $R$ , of the CIC Gaussian smoothed field and the WF reconstruction of the target data, of the BGc estimated data and of the observed data. In addition, the mean and the standard deviation around the mean of the moments of the BGc estimators of an ensemble of 10 errors realizations are shown as well. The monopole moment of the CIC and of the target data are robustly recovered for depth exceeding  $\sim 70h^{-1}\text{Mpc}$ . At smaller distances some deviations are found between the reconstructions from the target data and the BGc estimated data, and between these and the underlying CIC field. The dipole moment, namely the bulk velocity, is faithfully recovered across  $10 \lesssim R \lesssim 150h^{-1}\text{Mpc}$ .

Fig. 11 shows the cosmic variance around the 10 different mock observers as well as the errors variance, so as to gain further insight into the estimation of the monopole and dipole moments. It



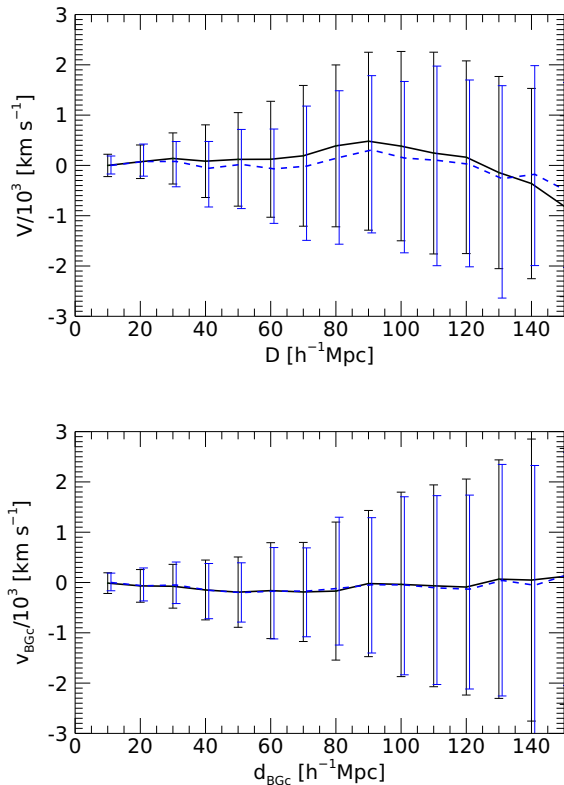


**Figure 8.** Mean (black, solid line) and median (blue, dashed line) of the observed velocity ( $V$ ) vs the observed distance ( $D$ , upper panel) and the estimated velocity ( $v_{BGc}$ ) vs the estimated distance ( $d_{BGc}$ , lower panel). (Same notations as in Fig. 6.)

shows the mean and scatter of the moments taken over the CIC fields around the mock observers and of the BGc data of the 10 different errors realizations around the 10 different observers. For both moments the cosmic + errors variance of the WF/BGc fields agrees virtually perfectly with the cosmic variance over the CIC fields. Comparison Figs. 10 and 11 shows that the cosmic variance dwarfs the variance due to the ‘observational’ errors.

The monopole moment discrepancy between the CIC, the target WF field and the WF/BGc fields (Fig. 10) can be partially attributed to the inherent nonlinearity of the CIC field. The approximate agreement between the target field and the WF/BGc reconstructions suggests that the BGc is doing well in removing the lognormal bias. The moments of the WF of the uncorrected ‘observed’ velocities are clearly misrepresenting the underlying field for  $R \gtrsim 50 h^{-1} \text{Mpc}$ .

## 7 A CLOSER LOOK AT THE ESTIMATION OF THE VELOCITIES

The mathematical expressions for the BGc estimated distances and velocities, Eqs. 23 and 36 consist of two terms - the first is the median of the relevant lognormal distribution and the other is its Gaussianization. Centralizing the resulting normal distribution on the median removes the biased mean value introduced by the log-

normal transformation (Eqs. 11 and 25) It is interesting to separate these two ingredients of the BGc procedure and check how they affect the WF reconstruction.

This is done here by constructing from a data set made of the BGc estimated velocities and velocities defined by

$$v_{m-shift} = (V|z)_{med}. \quad (38)$$

Namely, the Gaussianization term is omitted from Eq. 36 and the estimated velocities,  $v_{m-shift}$ , are set to the median of the lognormal distribution. Fig. 12 depicts the monopole and dipole moments of the WF reconstruction of the BGc estimated distances and velocities and of the  $v_{m-shift}$  data. The cases of the the WF reconstruction from the ideal  $V_{Gauss}$  target data and Gaussian smoothed ( $R_s = 5h^{-1} \text{Mpc}$  kernel) CIC are shown for reference. The dipole moment is less sensitive to the different data sets used here compared with the monopole moment. The dipole moments of the BGc (distances and velocities) and the  $V_{Gauss}$  data sets are virtually identical (for  $R \geq 20h^{-1} \text{Mpc}$ ) all the way to the edge of the data. The  $v_{m-shift}$  case overestimate the bulk velocity of the target  $V_{Gauss}$  by  $\sim 7\%$  at  $R \sim 60h^{-1} \text{Mpc}$ . As for the monopole moment, one finds very close agreement between the BGc,  $V_{Gauss}$  and the CIC cases, while the  $v_{m-shift}$  exhibits an offset of roughly  $-0.02$  for  $R \gtrsim 60h^{-1} \text{Mpc}$ . Such an offset corresponds to an overestimation of the value of Hubble’s constant by roughly  $1.5 \text{ km s}^{-1} \text{Mpc}^{-1}$ .

We conclude here that both ingredients in the BGc estimation of the velocities - the correction of the mean by the median and the Gaussianization - are essential for getting an unbiased estimator of the input velocities for the WF reconstruction.

## 8 ESTIMATION OF THE HUBBLE CONSTANT: MOCK CATALOGS

The simulation was run within the framework of the standard  $\Lambda \text{CDM}$  model and its cosmological parameters - in particular  $H_0^{\Lambda \text{CDM}} = 67.7 \text{ km s}^{-1} \text{Mpc}^{-1}$  was used. We set ourselves here to study the derived  $H_0$  from each CF3-like mock catalogs, constructed to sample the cosmic and errors variances. Four distinct classes of estimated  $H_0$  are used here: **a.**  $H_0^{\text{Nbody}}$  - the value estimated from the ‘clean’ data (i.e no errors added); **b.**  $H_0^{\text{obs}}$  - the value estimated from the observed data; **c.**  $H_0^{\text{BGc}}$  - the value estimated from the BGc corrected data; **d.**  $H_0^{\text{mean}}$  - the value estimated from the BGc corrected data, for which the Gaussianization of the distances is performed around the mean of the distribution. Namely, in Eq. 36  $(D|z)_{med}$  is replaced by the mean distance of the data points of the  $z$  subsample. The rationale behind the  $H_0^{\text{mean}}$  estimation is that the aim here is to overcome the scatter induced by the peculiar velocities around the observed redshift.

The Hubble constant is estimated here by linear regression over the distance-redshift scatter, in which both distances and redshift uncertainties are considered, and over all data points in the range of  $20 \leq d_z \leq 150 h^{-1} \text{Mpc}$ . The lower limit of the distance range has been chosen to correspond to that used for the case of the actual CF3 catalog, so as to exclude the effect of the Virgo cluster. The upper limit coincides with the range over which the BGc is applied. The formal statistical errors of the linear regression are very small in all case ( $\lesssim 0.1 \text{ km s}^{-1} \text{Mpc}^{-1}$ ) and are ignored here. The

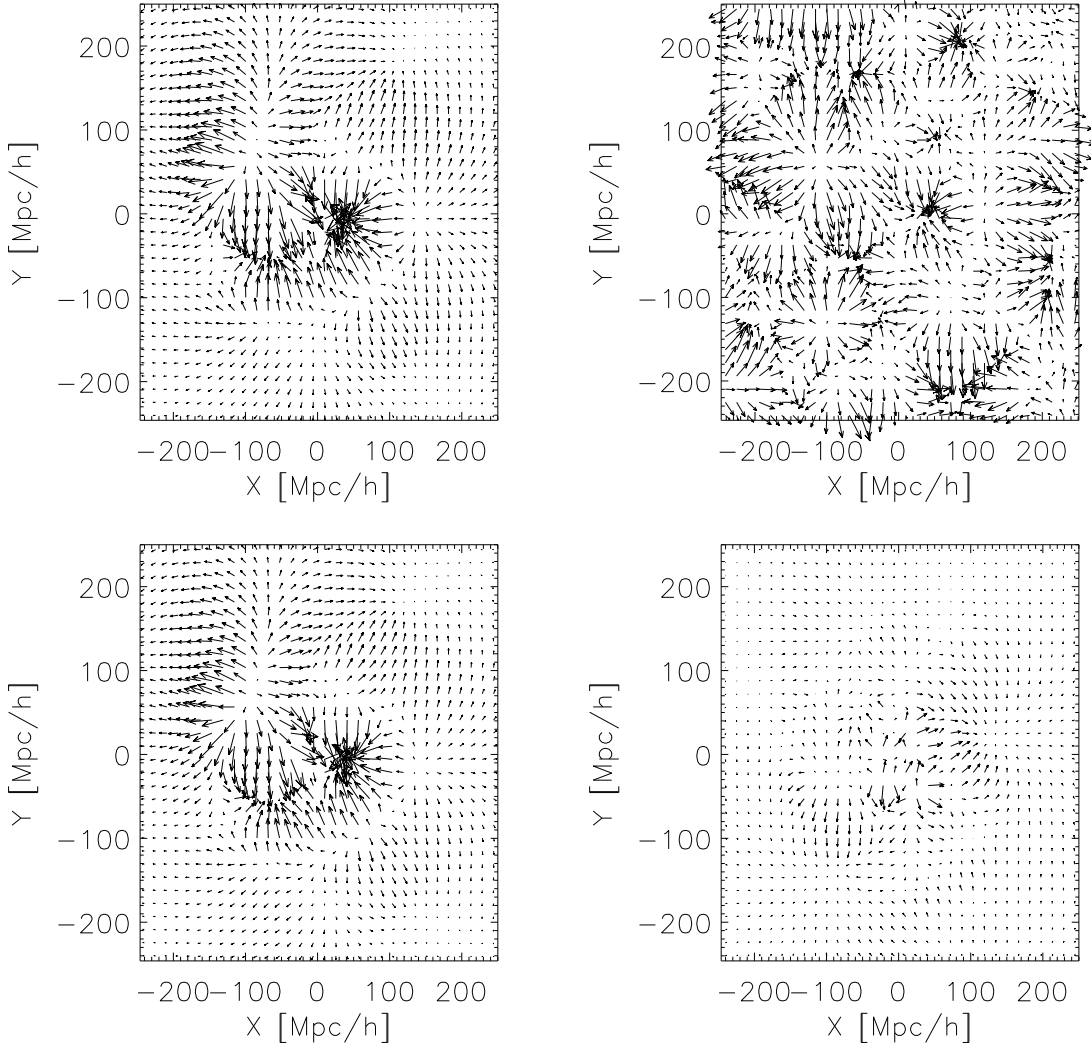


**Figure 9.** Visualization of flow fields: a. The target WF reconstructed from the  $V_{Gauss}$  data (see text) that is used here as a benchmark (upper-left panel) and the CIC velocity field, Gaussian smoothed with a  $5h^{-1}\text{Mpc}$  kernel (upper-right panel, the velocity arrows length is scaled down by a factor of 2 of the one used in the WF cases ). b. The WF reconstruction from the BGc estimated data (lower-left panel) and its residual of the WF reconstruction from the  $V_{Gauss}$  (lower-right panel). The flow fields are evaluated at the mock Supergalactic Plane.

results are summarized in Table 1 and are visually presented in the following figures: **a.** The error variance of the residual of the estimated  $H_0$  from the assumed  $H_0^{\text{ACDM}}$  of the simulation (Fig. 13); **b.** The cosmic variance of the residual of the estimated  $H_0$  from  $H_0^{\text{Nbody}}$  (Fig. 14); **c.** The error variance of the residual of the estimated  $H_0$  from  $H_0^{\text{Nbody}}$  (Fig. 15). Here the estimated values of  $H_0$  correspond to  $H_0^{\text{obs}}$ ,  $H_0^{\text{BGc}}$  and  $H_0^{\text{mean}}$ . The cosmic variance refers to the variance with respect to the different mock observers that are randomly scattered within the computational box of the simulation and the error variance corresponds to the scatter of the different realizations of the mock observational errors.

The fact that all the different estimators of  $H_0$  yield an estimate that is within  $\approx \pm 1.0$  with a scatter of  $\approx \pm 1.0 \text{ km s}^{-1} \text{ Mpc}^{-1}$  from  $H_0^{\text{ACDM}}$  is comforting. The finding that  $H_0^{\text{obs}} - H_0^{\text{ACDM}} = 0.1 \pm 1.2 \text{ km s}^{-1} \text{ Mpc}^{-1}$ , where the variance includes both the cosmic and the error variance, might seem surprising given there is some similarity between the ways the monopole term of the ve-

locity field and the  $H_0$  are constructed, hence in light of the gross discrepancy between the monopole term of the uncorrected data (distances and velocities) and the CIC ('true') one the lack of such discrepancy with regard to the different estimates of  $H_0$  might appear surprising. But one should recall that the 'uncorrected'  $H_0$  is derived essentially by linear regression of the uncorrected velocities on the redshifts. The bias of the scatter of the velocities around the redshifts is much smaller than that of the velocities around the distances, as manifested by the dotted-red curve of Fig. 10. The curve shows that at  $R = 150h^{-1}\text{Mpc}$  the mean value of the monopole term is  $\sim 3.0\%$ , namely  $\nabla \cdot \vec{v}/H_0 \sim -0.03$ . Assuming statistical anisotropy of the peculiar velocity field on the scale of the full CF3 data one expects the value of  $H_0$  derived from that WF reconstructed velocity field to be deficient by roughly a third of that value, i.e.  $\sim 1.0\%$ . Indeed, from Table 1 one infers that  $(H_0^{\text{obs}} - H_0^{\text{Nbody}})/H_0^{\text{Nbody}} = -0.013 \pm 0.003$  - consistent with the WF reconstructed from the observed uncorrected velocities and the redshift distances.

$H_0^{\text{Nbody}} - H_0$	$H_0^{\text{obs}} - H_0$	$H_0^{\text{mean}} - H_0$	$H_0^{\text{BGc}} - H_0$	$H_0^{\text{obs}} - H_0^{\text{Nbody}}$	$H_0^{\text{mean}} - H_0^{\text{Nbody}}$	$H_0^{\text{BGc}} - H_0^{\text{Nbody}}$
	$0.1 \pm 1.3 \pm 0.2$	$0.2 \pm 1.0 \pm 0.4$	$1.6 \pm 1.1 \pm 0.4$	$-0.9 \pm 0.1 \pm 0.2$	$-0.8 \pm 0.5 \pm 0.6$	$0.6 \pm 0.6 \pm 0.4$
$1.0 \pm 1.2$	$0.1 \pm 1.3$	$0.2 \pm 1.1$	$1.6 \pm 1.2$	$-0.9 \pm 0.2$	$-0.8 \pm 0.8$	$0.6 \pm 0.7$

**Table 1.** The mean and standard deviation of the residual of  $H_0^{\text{obs}}$  and of  $H_0^{\text{BGc}}$  from the actual  $H_0^{\text{CDM}}$  and from the actual value measure by each mock observer  $H_0^{\text{Nbody}}$ : The upper observed presents separately the scatter due to the cosmic variance (1st uncertainty) and the error variance (2nd uncertainty). The lower observed shows the total uncertainty. (All values are in units of  $\text{km s}^{-1}\text{Mpc}^{-1}$ .)

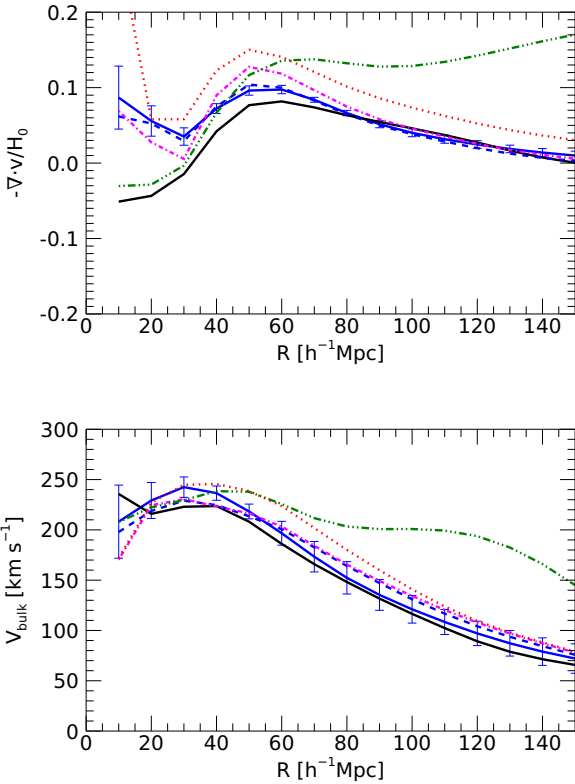


**Figure 10.** The monopole (upper panel) and the dipole (namely the bulk velocity, lower panel) moments of the velocity field of the: a. CIC smoothed velocity field of the simulation (black); b. The WF reconstruction from the BGc corrected data of a single errors realization (dashed blue); c. The mean and the standard deviation of of the WF reconstruction from the an ensemble of BGc data of 10 errors realizations (solid, blue); d. The WF reconstruction from the data with exact distances and Gaussian errors on the velocities ( $V_{\text{Gauss}}$ ) of the same errors realization (dot-dashed magenta); e. The WF reconstruction from the ‘observed’ data (dot-dot-dashed green). f. The WF reconstruction from the redshift distance and the ‘observed’ uncorrected data (dotted, red). The main lesson to take here is the gross discrepancy between the multipoles of WF of the uncorrected data and the CIC and the CIC ‘true’ field beyond  $\approx 50h^{-1}\text{Mpc}$ . This stands in sharp contrast with the good agreement for the WF of the BGc corrected data and the CIC cases.

## 9 COSMICFLOWS-3 DATA: BGC

Fig 16 presents the CF3 data. Its upper panel shows the distribution of the observed peculiar radial velocities vs the observed distances and its lower panel presents that distribution for the BGc estimators. The bias and the non-Gaussianity of the distribution of the observed velocities are clearly manifested. These are eliminated by the BGc estimators, the former by the gross deviation of the mean

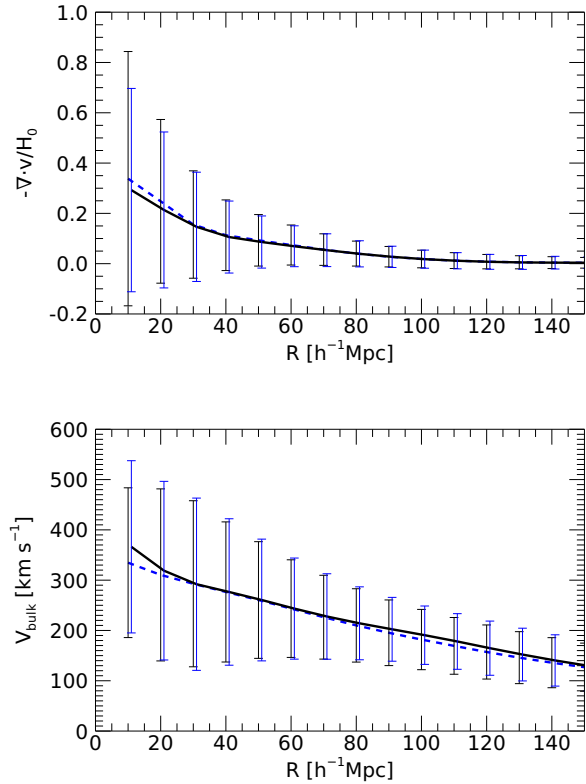


**Figure 11.** The mean and scatter around the mean of the monopole (upper panel) and the dipole (namely the bulk velocity, lower panel) moments of: a. The CIC smoothed velocity fields of the ensemble of mock observers (cosmic variance; black). b. The WF reconstructed velocity fields from the ensemble of 100 mock catalogs (cosmic and error variance, blue).

of the velocities from the expected null value and the latter from significant difference between the mean and the median of the velocities in the radial bins.

The estimated Hubble constant from the CF3 data is  $H_0 = 75.8 \pm 0.1 \pm 1.0 \pm 0.4 \text{ km s}^{-1}\text{Mpc}^{-1}$ , where the first uncertainty (0.1) corresponds to the formal statistical error, the 2nd (1.0) to the cosmic variance and the 3rd ( $0.4 \text{ km s}^{-1}\text{Mpc}^{-1}$ ) to the error variance. The estimation of the uncertainties due to the cosmic and error variances are taken from the analysis of the mock catalogs. Tully et al. (2016) estimation, based on the analysis of the peculiar velocities monopole term, is  $H_0 = 75 \pm 2 \text{ km s}^{-1}\text{Mpc}^{-1}$ .

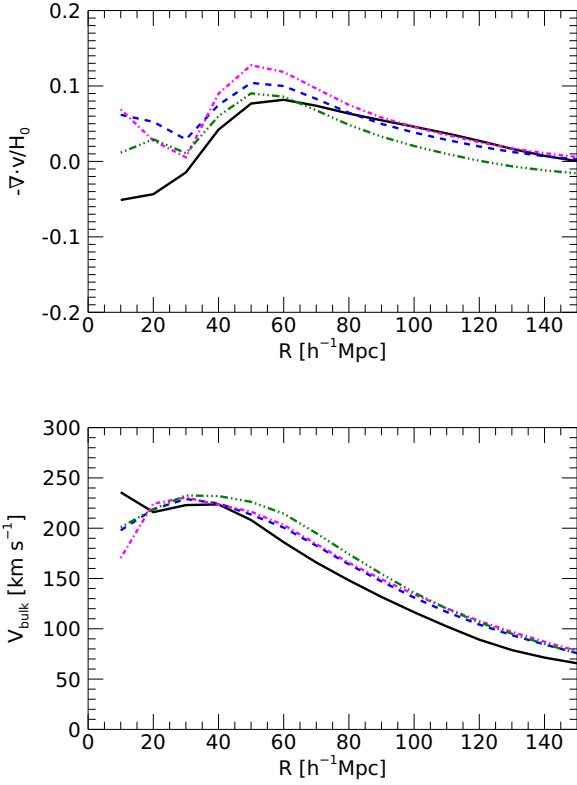


**Figure 12.** The monopole (upper panel) and the dipole (lower panel) moments of the WF reconstructed velocity fields from the following data sets: a. BGc (blue, dashed); b. The VGauss target ideal data (magenta, dot-dashed); c. BGc distances ( $d_{BGc}$ ) and observed velocities shifted by the lognormal bias (green, dot-dot-dashed); The moments of the Gaussian smoothed CIC velocity field is presented for reference (black, solid).

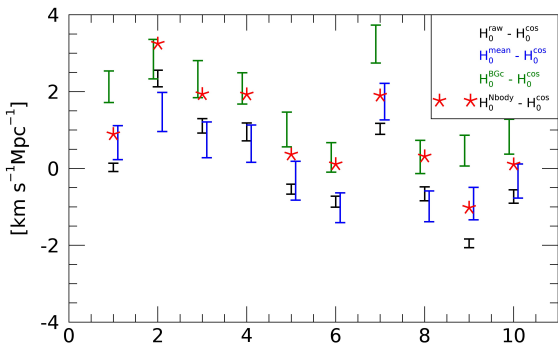


**Figure 13.** Error variance: The mean and scatter of the residual of the estimated values of  $H_0$  from the  $\Lambda$ CDM assumed value of  $H_0^{\Lambda\text{CDM}} = 67.7 \text{ km s}^{-1} \text{ Mpc}^{-1}$  for each one of the mock CF3 observer (denoted by horizontal axis). Three case are considered here:  $H_0^{\text{obs}}$  (black),  $H_0^{\text{mean}}$  (blue) and  $H_0^{\text{BGc}}$  (green). The red asterisk symbols represent the  $H_0^{\text{Nbody}}$  of the individual mock observers. The horizontal axis labels the different mock catalogs.

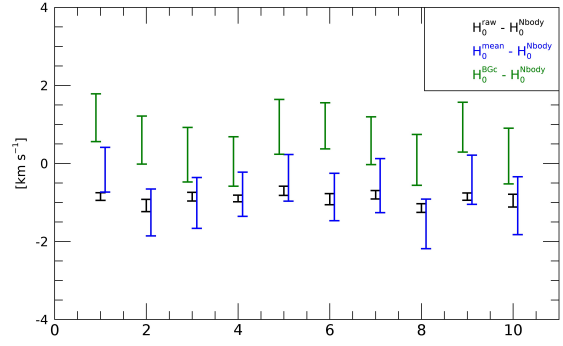


**Figure 14.** Cosmic variance: The mean and scatter of the residual of the estimated values of  $H_0$  from the actual  $H_0^{\text{Nbody}}$  for each one of the different errors realization (denoted by horizontal axis). Three case are considered here:  $H_0^{\text{obs}}$  (black),  $H_0^{\text{mean}}$  (blue) and  $H_0^{\text{BGc}}$  (green). The horizontal axis labels the different mock catalogs.

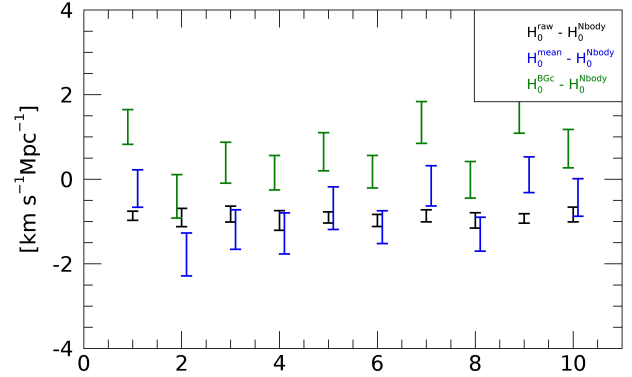


**Figure 15.** Error variance: The mean and scatter of the residual of the estimated values of  $H_0$  from the actual  $H_0^{\text{Nbody}}$  for each one of the mock CF3 observer (denoted by horizontal axis). Three case are considered here:  $H_0^{\text{obs}}$  (black),  $H_0^{\text{mean}}$  (blue) and  $H_0^{\text{BGc}}$  (green). The horizontal axis labels the different mock catalogs.

## 10 DISCUSSION

Surveys of peculiar velocities of galaxies are actually surveys of their luminosity distances and redshifts and the proper distances and peculiar velocities are derived quantities. Within that context the redshifts are (relatively) easily obtained and are accurately known. Estimating distances from observed astronomical data is challenging. Going beyond the formidable challenge of the zero-point calibration of the various distance indicator one faces the issue that the observational errors are Gaussian distributed on the distance moduli and thereby are lognormal on the actual distances and on the peculiar velocities. This is the lognormal bias. A scheme, the bias Gaussianization correction (BGc), is presented here to undo that bias. This is done by constructing a subsample of data points at a given redshift and Gaussianizing the distribution of their distances and of their peculiar velocities, while retaining the medians of these distribution. Consequently, the basic relation between the Hubble velocity, hence distance, peculiar velocity and the redshift

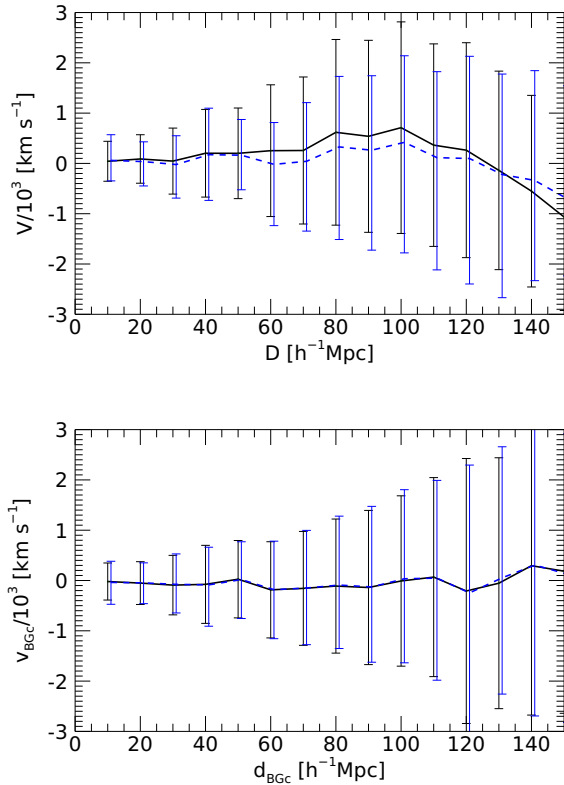


**Figure 16.** Mean (black, solid line) and median (blue, dashed line) of the CF3 observed velocity ( $V$ ) vs the observed distance ( $D$ , upper panel) and of the estimated velocity ( $v_{BGc}$ ) vs the estimated distance ( $d_{BGc}$ , lower panel). (Same notations as in Fig. 6.)

holds statistically, in the sense of mean values, per the given subsample. It is the invariance of the median under the Gaussianization transformation which preserves the underlying monopole moment of the velocity field and suppresses the lognormal bias.

Some of the robust conclusions to be drawn from the paper are: a. The BGc algorithm eliminates the lognormal bias; b. In the context of the WF/CRs reconstruction the BGc corrected data well approximates the case of an ideal data made of exact distances and normal errors added to the peculiar velocities; c. The dipole moment, i.e. the bulk velocity, of the WF reconstructed velocity field from the BGc data closely recovers the dipole moment of the underlying velocity field all the way to the edge of the data.; d. The monopole moment, namely the mean of appropriately scaled divergence of the velocity field, of the WF/BGc reconstruction is a good proxy to the true monopole from  $R \sim 70 h^{-1} \text{Mpc}$  to the edge of the data; e. The error variance of the monopole and dipole moments is negligible compared with the cosmic variance; f. The mean and variance of the monopole and dipole moments of the WF/BGc reconstructed velocity field are in a good agreement with the mean and cosmic variance derived from the numerical simulation.

Our main motivation for the introduction of the BGc algorithm has been the construction of CF3 data of unbiased distances and velocities - one that can be used for cosmological parameters estimation and in particular for the reconstruction of the large scale structure of the nearby universe. i.e. the local density and 3D velocity

fields. More specifically, we looked for an unbiased estimator of the CF3 data so as to use it for an unbiased WF/CRs reconstruction of the local universe. The WF/CRs reconstruction from the BGc corrected CF3 data is to be presented elsewhere (Hoffman et al, in prep).

The BGc handles only issues related to the lognormal bias. It does not address potential biases and uncertainties associated with the zero-point calibration of the different data sets that make the CF3 data. No attempt is made here to address issues related to the zero-point calibration and it is taken at its face value.

The main caveat to be concerned with the BGc is that it acts to correct the 1-point PDF of the velocities without any reference to the 2-point distribution function. This can be justified by the fact that the amplitudes of the observed velocities, apart from the very nearby data points, are heavily dominated by the uncorrelated distance errors. The affect of that caveat is investigated in our upcoming WF/CRs paper.

Of particular interest is the comparison of the BGc treatment of the bias with that of the Bayesian MCMC method of Graziani et al. (2019). Both methods have been applied to the CF3 mock catalogs and are compared by means of their reconstructed density and velocity fields (Valade et al, in prep). Preliminary results indicate an overall good agreement between the two - they both recover the ‘same (mock) universe’. Yet, some subtle differences exist and they are currently being explored.

## DATA AVAILABILITY STATEMENT

The modifications to observed *Cosmicflows-3* distances resulting from the BGc analysis are compiled in a file hosted at the *Extragalactic Distance Database* (<http://edd.ifa.hawaii.edu>), in the section *Summary Distances*, labeled *CF3 Modelled Group Distances*. The file includes BGc distances and inferred peculiar velocities and, for comparison, the equivalent information from the Graziani et al. (2019) Bayesian MCMC analysis and the directly observed values.

## ACKNOWLEDGEMENTS

This work has been done within the framework of the Constrained Local UniversE Simulations (CLUES) simulations. YH has been partially supported by the Israel Science Foundation grant ISF 1358/18. AN has been supported by the Israel Science Foundation grant ISF 936/18. NIL & AV acknowledge financial support of the Project IDEXLYON at the University of Lyon under the Investments for the Future Program (ANR-16-IDEX-0005). RBT was supported in the development of the Cosmicflows-3 collection of distances by US National Science Foundation award AST09-08846 and NASA award NNX12AE70G.

## REFERENCES

- Courtois H. M., Hoffman Y., Tully R. B., Gottlöber S., 2012, *ApJ*, 744, 43
- Courtois H. M., Pomarède D., Tully R. B., Hoffman Y., Courtois D., 2013, *AJ*, 146, 69
- da Costa L. N., Freudling W., Wegner G., Giovanelli R., Haynes M. P., Salzer J. J., 1996, *ApJL*, 468, L5
- Davis T. M., Scrimgeour M. I., 2014, *MNRAS*, 442, 1117
- Dekel A., Bertschinger E., Faber S. M., 1990, *ApJ*, 364, 349
- Dekel A., Bertschinger E., Yahil A., Strauss M. A., Davis M., Huchra J. P., 1993, *ApJ*, 412, 1
- Forero-Romero J. E., Hoffman Y., Yepes G., Gottlöber S., Piontek R., Klypin A., Steinmetz M., 2011, *MNRAS*, 417, 1434
- Graziani R., Courtois H. M., Lavaux G., Hoffman Y., Tully R. B., Copin Y., Pomarède D., 2019, *MNRAS*, 488, 5438
- Hoffman Y., Carlesi E., Pomarède D., Tully R. B., Courtois H. M., Gottlöber S., Libeskind N. I., Sorce J. G., Yepes G., 2018, *Nature Astronomy*, 2, 680
- Hoffman Y., Martinez-Vaquero L. A., Yepes G., Gottlöber S., 2008, *MNRAS*, 386, 390
- Hoffman Y., Pomarède D., Tully R. B., Courtois H. M., 2017, *Nature Astronomy*, 1, 0036
- Hoffman Y., Ribak E., 1991, *ApJL*, 380, L5
- Lavaux G., 2016, *MNRAS*, 457, 172
- Lilje P. B., Yahil A., Jones B. J. T., 1986, *ApJ*, 307, 91
- Lynden-Bell D., 1992, in *Statistical Challenges in Modern Astronomy Eddington-Malmquist bias, streaming motions, and the distribution of galaxies.* pp 201–220
- Lynden-Bell D., Faber S. M., Burstein D., Davies R. L., Dressler A., Terlevich R. J., Wegner G., 1988, *ApJ*, 326, 19
- Malmquist G. K., 1920, *Meddelanden fran Lunds Astronomiska Observatorium Serie II*, 22, 3
- Malmquist K. G., 1924, *Meddelanden fran Lunds Astronomiska Observatorium Serie II*, 32, 3
- Masters K. L., Springob C. M., Haynes M. P., Giovanelli R., 2006, *ApJ*, 653, 861
- Nusser A., 2017, *MNRAS*, 470, 445
- Nusser A., Davis M., 1995, *MNRAS*, 276, 1391
- Nusser A., Davis M., 2011, *ApJ*, 736, 93
- Ocvirk P., Aubert D., Sorce J. G., Shapiro P. R., Deparis N., Dawoodbhoy T., Lewis J., Teyssier R., Yepes G., Gottlöber S., Ahn K., Iliev I. T., Hoffman Y., 2020, *MNRAS*, 496, 4087
- Peebles P. J. E., 1980, *The large-scale structure of the universe*
- Peery S., Watkins R., Feldman H. A., 2018, *MNRAS*, 481, 1368
- Planck Collaboration 2014, *A&A*, 571, A16
- Pomarède D., Hoffman Y., Courtois H. M., Tully R. B., 2017, *ApJ*, 845, 55
- Pomarède D., Tully R. B., Graziani R., Courtois H. M., Hoffman Y., Lezmy J., 2020, *ApJ*, 897, 133
- Sorce J. G., 2015, *MNRAS*, 450, 2644
- Sorce J. G., Gottlöber S., Yepes G., Hoffman Y., Courtois H. M., Steinmetz M., Tully R. B., Pomarède D., Carlesi E., 2016, *MNRAS*, 455, 2078
- Springob C. M., Magoulas C., Colless M., Mould J., Erdoğdu P., Jones D. H., Lucey J. R., Campbell L., Fluke C. J., 2014, *MNRAS*, 445, 2677
- Strauss M. A., Willick J. A., 1995, *Phys. Rep.*, 261, 271
- Tully R. B., Courtois H., Hoffman Y., Pomarède D., 2014, *Nature*, 513, 71
- Tully R. B., Courtois H. M., Dolphin A. E., Fisher J. R., Héraudeau P., Jacobs B. A., Karachentsev I. D., Makarov D., Makarova L., Mitronova S., Rizzi L., Shaya E. J., Sorce J. G., Wu P.-F., 2013, *AJ*, 146, 86
- Tully R. B., Courtois H. M., Sorce J. G., 2016, *AJ*, 152, 50
- Tully R. B., Fisher J. R., 1977, *A&A*, 54, 661
- Tully R. B., Shaya E. J., Karachentsev I. D., Courtois H. M., Kocovski D. D., Rizzi L., Peel A., 2008, *ApJ*, 676, 184
- Watkins R., Feldman H. A., 2015, *MNRAS*, 450, 1868
- Weinberg S., 2008, *Cosmology*
- Yepes G., Gottlöber S., Hoffman Y., 2014, *New Astronomy Reviews*, 58, 1
- Zaroubi S., Bernardi M., da Costa L. N., Hoffman Y., Alonso M. V., Wegner G., Willmer C. N. A., Pellegrini P. S., 2001, *MNRAS*, 326, 375
- Zaroubi S., Hoffman Y., Dekel A., 1999, *ApJ*, 520, 413
- Zaroubi S., Hoffman Y., Fisher K. B., Lahav O., 1995, *ApJ*, 449, 446

This paper has been typeset from a  $\text{\TeX}/\text{\LaTeX}$  file prepared by the author.